

**Electron kinetic effects on interferometry, polarimetry and Thomson scattering measurements in burning plasmas (invited)a)**

V. V. Mirnov, D. L. Brower, D. J. Den Hartog, W. X. Ding, J. Duff, and E. Parke

Citation: [Review of Scientific Instruments](#) **85**, 11D302 (2014); doi: 10.1063/1.4891176

View online: <http://dx.doi.org/10.1063/1.4891176>

View Table of Contents: <http://scitation.aip.org/content/aip/journal/rsi/85/11?ver=pdfcov>

Published by the [AIP Publishing](#)

---

**Articles you may be interested in**

[First measurement of time evolution of electron temperature profiles with Nd:YAG Thomson scattering system on Heliotron Ja\)](#)

Rev. Sci. Instrum. **85**, 11D819 (2014); 10.1063/1.4890255

[Short-interval multi-laser Thomson scattering measurements of hydrogen pellet ablation in LHDA\)](#)

Rev. Sci. Instrum. **85**, 11D822 (2014); 10.1063/1.4890251

[Collective Thomson scattering of a high power electron cyclotron resonance heating beam in LHD \(invited\)a\)](#)

Rev. Sci. Instrum. **81**, 10D535 (2010); 10.1063/1.3481165

[Advanced Interferometry Techniques for Burning Plasmas](#)

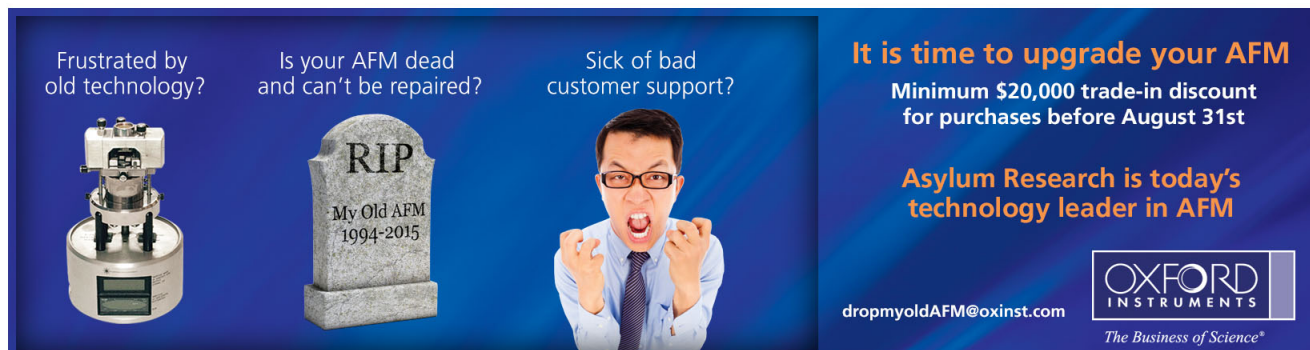
AIP Conf. Proc. **988**, 92 (2008); 10.1063/1.2905125

[Finite electron temperature effects on interferometric and polarimetric measurements in fusion plasmas](#)

Phys. Plasmas **14**, 102105 (2007); 10.1063/1.2790886

---

Frustrated by old technology?      Is your AFM dead and can't be repaired?      Sick of bad customer support?



**It is time to upgrade your AFM**  
Minimum \$20,000 trade-in discount for purchases before August 31st

**Asylum Research is today's technology leader in AFM**

[dropmyoldAFM@oxinst.com](mailto:dropmyoldAFM@oxinst.com)

**OXFORD INSTRUMENTS**  
The Business of Science®

# Electron kinetic effects on interferometry, polarimetry and Thomson scattering measurements in burning plasmas (invited)<sup>a)</sup>

V. V. Mirnov,<sup>1</sup> D. L. Brower,<sup>2</sup> D. J. Den Hartog,<sup>1</sup> W. X. Ding,<sup>2</sup> J. Duff,<sup>1</sup> and E. Parke<sup>1</sup>

<sup>1</sup>*Physics Department, University of Wisconsin - Madison and the Center for Magnetic Self-Organization in Laboratory and Astrophysical Plasmas, Madison, Wisconsin 53706, USA*

<sup>2</sup>*Department of Physics and Astronomy, University of California Los Angeles, Los Angeles, California 90095, USA*

(Presented 2 June 2014; received 29 May 2014; accepted 12 July 2014; published online 5 August 2014)

At anticipated high electron temperatures in ITER, the effects of electron thermal motion on Thomson scattering (TS), toroidal interferometer/polarimeter (TIP), and poloidal polarimeter (PoPola) diagnostics will be significant and must be accurately treated. The precision of the previous lowest order linear in  $\tau = T_e/m_e c^2$  model may be insufficient; we present a more precise model with  $\tau^2$ -order corrections to satisfy the high accuracy required for ITER TIP and PoPola diagnostics. The linear model is extended from Maxwellian to a more general class of anisotropic electron distributions that allows us to take into account distortions caused by equilibrium current, ECRH, and RF current drive effects. The classical problem of the degree of polarization of incoherent Thomson scattered radiation is solved analytically exactly without any approximations for the full range of incident polarizations, scattering angles, and electron thermal motion from non-relativistic to ultra-relativistic. The results are discussed in the context of the possible use of the polarization properties of Thomson scattered light as a method of  $T_e$  measurement relevant to ITER operational scenarios. © 2014 AIP Publishing LLC. [<http://dx.doi.org/10.1063/1.4891176>]

## I. INTRODUCTION

Toroidal interferometry/polarimetry (TIP), poloidal polarimetry (PoPola), and Thomson scattering (TS) are major optical diagnostics being designed and developed for ITER. Since they are needed for basic machine operation as well as physics studies, accurate measurements are required to meet ITER operational goals. Fundamentally, each of these diagnostics relies upon a sophisticated quantitative understanding of the electron response to laser light propagating through a burning plasma. Improvements in this understanding are being used to guide and constrain the design of these diagnostics, and, once they are operational, will be used to improve measurement accuracy. These improvements will enable proper application of diagnostic measurements to direct real-time feedback control of ITER device operation. The primary focus of our work is to examine the effects of electron thermal motion on the refractive indices and polarization of high-frequency electromagnetic waves (specifically laser light, both directed and scattered).

The magnetized plasma exhibits birefringence, and two orthogonal states of wave polarization with different refractive indices are present. Important consequences of plasma birefringence are the Faraday (FR) effect of rotation of the polarization plane and the Cotton-Mouton effect (CM) leading to both rotation and deformation of the polarization ellipse.<sup>1</sup> For the waves propagating in the direction of the incident laser beam and used for the purposes of interferometry and po-

larimetry (I/P), we calculate electron thermal corrections to the interferometric phase and polarization state of the light (FR and CM polarimetry). Our initial results<sup>2</sup> were obtained from a linear in  $\tau = T_e/m_e c^2 \ll 1$  isotropic electron temperature model. They have already been included in the error analysis and design projections of the ITER TIP and PoPola systems.<sup>3,4</sup> The new findings are: (1) the precision of the lowest order linear in  $\tau$  model may be insufficient; we present a more precise model with  $\tau^2$ -order corrections to satisfy the high accuracy required for ITER TIP and PoPola diagnostics and (2) the linear model is extended from Maxwellian to a more general class of anisotropic electron distributions. This allows us to take into account a shift of distribution due to mean parallel electron drift velocity (current) and effects of temperature anisotropy caused by ECRH or RF current drive systems. The shift mechanism is discussed in relation to the possibility of Fizeau interferometry/polarimetry to measure the equilibrium plasma current density.

Interaction of the laser beam with plasma causes light to scatter away from the direction of the incident light. This low intensity Thomson scattered light is used for electron temperature and density measurements. In application to this diagnostic, we calculate the degree of polarization of incoherent Thomson scattered laser light analytically exactly without any approximations for the full range of incident polarizations, scattering angles, and electron thermal motion from non-relativistic to ultra-relativistic. The results are discussed in the context of the proposal<sup>5</sup> to use the polarization properties of Thomson scattered light as a method of  $T_e$  measurement relevant to ITER operational scenarios. The purpose of this paper is to review recent theoretical results in support of optical diagnostics in burning plasmas. The progress achieved

<sup>a)</sup>Invited paper, published as part of the Proceedings of the 20th Topical Conference on High-Temperature Plasma Diagnostics, Atlanta, Georgia, USA, June 2014.

in Thomson scattering analysis will be described first below, followed by interferometry and polarimetry.

## II. THOMSON SCATTERING

Incoherent Thomson scattering is routinely used for electron temperature measurement, with  $T_e$  proportional to the width of the scattered spectrum.<sup>6</sup> The scattering process changes the polarization of the light, an effect that becomes large in high-temperature burning plasmas and is typically described by the relativistic depolarization factor  $q$  (see Ref. 6). This factor quantifies the reduction of scattered spectral intensity caused by relativistic terms  $\propto v_e^2/c^2$  in the polarization part of the scattering operator. Although the reduction is referred to as depolarization, it is different from the common understanding of depolarization considered in our paper. Indeed, the aforementioned reduction of intensity takes place even for scattering on a single moving electron. In this case, the scattered electromagnetic wave has a Doppler-shifted frequency but still remains monochromatic and completely polarized. We analyze the superposition effect caused by a large number of randomly moving electrons. It results in broadening of the frequency spectrum and renders the scattered radiation partially polarized even though the incident light is fully polarized.

The loss of polarization is quantified by the *degree of polarization*  $P$ , or equivalently by the *degree of depolarization*  $D = 1 - P$ . The possibility of determining the plasma electron temperature by measuring the degree of depolarization was suggested in Ref. 5. If the degree of polarization dependence on electron temperature is accurately known from theory, the accuracy of such a diagnostic could potentially exceed that of the conventional spectrum-based TS method. Thus motivated, we revisited this topic to analyze whether polarization effects may be suitable for application to advanced TS diagnostics on ITER. In our analysis, we follow Ref. 7, with some important corrections and improvements. In particular, the finite transit time effect<sup>8</sup> is properly incorporated into the scattering operator. Another important improvement is optimal choice of the reference frame for averaging over velocity space. This allows derivation of an exact relativistic analytical expression for the degree of depolarization.<sup>9</sup>

Polarization properties of a non-monochromatic plane wave are characterized by the complex coherency matrix  $\mathbf{J}$ . The matrix is constructed from time averaged quadratic combinations of the field components and represented, in general, by four real quantities which can be equivalently expressed by four Stokes parameters or 4-component Stokes vector  $\mathbf{S}$

$$\mathbf{J} = \begin{pmatrix} \overline{E_x E_x^*} & \overline{E_x E_y^*} \\ \overline{E_y E_x^*} & \overline{E_y E_y^*} \end{pmatrix} = \frac{1}{2} \begin{pmatrix} S_0 + S_1 & S_2 + iS_3 \\ S_2 - iS_3 & S_0 - S_1 \end{pmatrix}.$$

The  $S_0$  component corresponds to the total intensity of the wave and the remaining components describe the polarization properties. For a purely monochromatic, fully polarized incident wave, the amplitudes and the phases of  $E_x$  and  $E_y$  are independent of time. In this case  $\det[\mathbf{J}] = 0$ , leading to the relationship  $S_0^2 = S_1^2 + S_2^2 + S_3^2$ . Correspondingly, the state of polarization of the incident laser light in TS experiments and the waves used for IP measurements are described by the re-

duced three-component unit Stokes vector  $\mathbf{s}_i = S_i/S_0$  ( $i = 1, 2, 3$ ). The vector  $\mathbf{s}$  is characterized by the azimuth (orientation angle) of the polarization ellipse  $0 \leq \psi < \pi$  (measured from the perpendicular to the scattering plane) and the ellipticity angle  $\chi = \pm \arctan(b_2/b_1)$  determined by the ratio of the minor and the major axis ( $-\pi/4 < \chi \leq \pi/4$ ). Then, the four-component Stokes vector of fully polarized incident laser light is expressed as  $\mathbf{S}^{(i)} = S_0(1, \cos 2\psi \cos 2\chi, \sin 2\psi \cos 2\chi, \sin 2\chi)$ .

A fully unpolarized wave (natural light) is characterized by  $S_1 = S_2 = S_3 = 0$ . Any partially polarized wave can be decomposed into completely unpolarized and polarized portions yielding the degrees of polarization/depolarization of the scattered radiation<sup>10</sup>

$$P = \frac{I_{pol}}{I_{tot}} = \frac{\sqrt{S_1^{(s)2} + S_2^{(s)2} + S_3^{(s)2}}}{S_0^{(s)}}, \quad D = 1 - P.$$

Making use of the definition of the Stokes vector allows us to obtain the  $4 \times 4$  Mueller matrix that describes the transformation of the Stokes vectors in the process of scattering on a single electron moving with an arbitrary velocity  $\mathbf{v}$ ,  $\mathbf{S}^{(s)} = \mathbf{M}^{(single)}(\mathbf{v}) \cdot \mathbf{S}^{(i)}$ . Time averaging is performed by integrating over the whole frequency range that removes a delta-function dependence on frequency in  $\mathbf{M}^{(single)}$ . This corresponds to the transition from the spectrum-based characteristics to the polarization analysis based on the total frequency integrated intensities. As the scattering is incoherent, the Stokes vector of the total scattered radiation is the sum of the Stokes vectors of radiation scattered by the separate electrons. The resulting effect is described by the Mueller matrix  $\mathbf{M}(\mu, \theta) = C\mathbf{m}(\mu, \theta)$  averaged over a relativistic Maxwellian distribution

$$\begin{aligned} m_{00} &= 1 + u^2 - 2G(\mu)(u^2 + 4u - 3) + (16/\mu^2)(1 - u)^2, \\ m_{01} &= m_{10} = 1 - u^2, \\ m_{11} &= 1 + u^2 + 2G(\mu)(u^2 - 4u + 1) + (12/\mu^2)(1 - u)^2, \\ m_{22} &= 2u - 4G(\mu)(u^2 - u + 1) - (12/\mu^2)(1 - u)^2, \\ m_{33} &= 2u - 4G(\mu)u(2u - 1) - (8/\mu^2)(1 - u)^2, \end{aligned}$$

while the constant factor  $C = r_0^2 N / 2r^2$ , where  $r_0$ ,  $r$  and  $N$  are the classical electron radius, the distance from the scattering volume to the point of observation (detector) and the total number of electrons inside the scattering volume, respectively (see definition of the dimensionless factor  $N$  in Sec. II D of Ref. 8). This large factor is important for the intensity of Thomson scattered radiation, but not included in Ref. 7. All integrations in  $\mathbf{m}$  are performed in analytical form yielding functions of the scattering angle,  $u = \cos \theta$ , and electron temperature via the factor  $\mu = m_e c^2 / T_e$  and function  $G(\mu) = K_1(\mu) / (\mu K_2(\mu))$ , where  $K_1$  and  $K_2$  are modified Bessel functions of the second kind. These matrix elements present an exact analytical solution for the state of polarization of incoherent Thomson scattering radiation. They are different from Ref. 7 where only the lowest order in  $\tau$  analytical results were obtained without the finite residence time effect taken into account (the incorrect weighting factor  $(1 - \beta_s)^{-6}$  instead of  $(1 - \beta_s)^{-5}$ ).

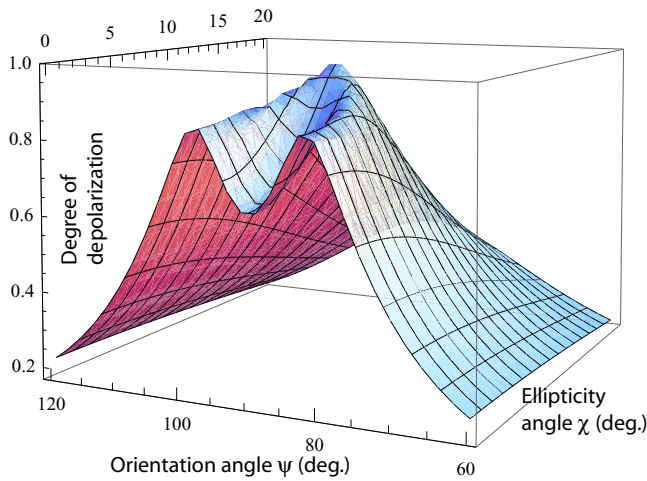


FIG. 1. Depolarization degree vs orientation and ellipticity angles  $\psi$  and  $\chi$  at  $\theta = 90^\circ$ ,  $T_e = 10$  keV. There is a local maximum of  $D$  at  $\psi \simeq 82^\circ$  and  $\chi = 0$  (linear polarization), but the absolute maximum is reached at  $\psi = 90^\circ$  and  $\chi \simeq 9^\circ$  (elliptical polarization).  $D$  is an even function of  $\cos \psi$  illustrated in this figure by plotting  $\psi > 90^\circ$ .

The degree of depolarization depends on  $T_e$ , scattering angle  $\theta$ , and polarization characteristics of the incident light  $\psi$  and  $\chi$ . One particular example illustrating a maxima of  $D$  as a function of  $\psi$  and  $\chi$  is shown in Fig. 1 for  $T_e = 10$  keV and  $\theta = 90^\circ$ . At any given  $\theta$  and  $T_e$ , extrema of  $D$  as a function of  $\psi$  and  $\chi$  are reached at the boundaries of the region  $0 \leq \psi \leq \pi/2$ ,  $0 \leq \chi \leq \pi/4$ . This allows us to find the absolute maximum  $D_{max}(T_e, \theta)$ , and minimum  $D_{min}(T_e, \theta)$ , with respect to all possible polarization states of the incident radiation, and to set upper and lower limits on  $D$  at given  $\theta$  and  $T_e$ . Quantitative pictures of the dependences of these two functions on  $T_e$  and  $\theta$  are shown in Figs. 2 and 3. A good test of correctness

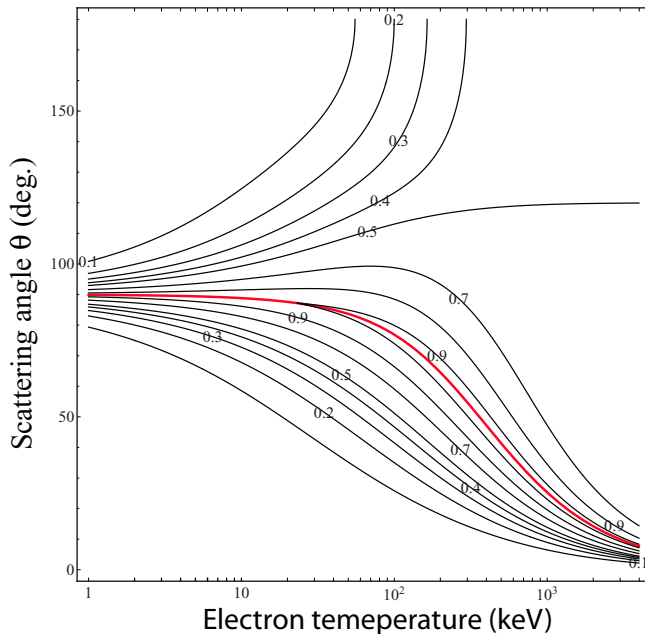


FIG. 2. Contour lines of the maximum value of the degree of depolarization  $D_{max}(T_e, \theta)$  (maximized with respect to all possible polarization states of the incident light). The red curve is a boundary in  $(T_e, \theta)$  space that determines which of the two maxima shown in Fig. 1 provides the absolute maximum.

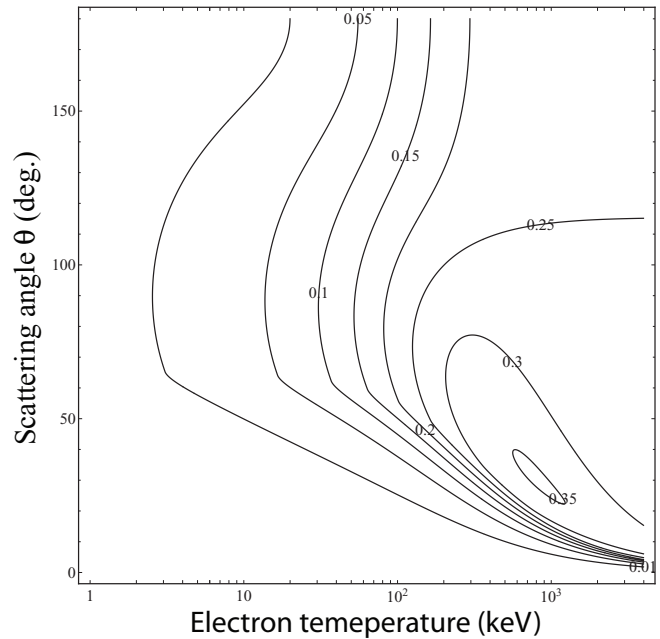


FIG. 3. Contour lines of the minimum value of the degree of depolarization  $D_{min}(T_e, \theta)$  (minimized with respect to all possible polarization states of the incident laser light).

of the matrix elements  $\mathbf{m}$  is that for all values of the variables  $0 \leq D < 1$ .

The planned ITER LIDAR TS system detects backscattered radiation at  $\theta \sim 180^\circ$ . For such backscattered light, the degree of depolarization is quadratic in  $\tau \ll 1$  and, therefore, small ( $\sim 3\% - 5\%$ ) at the temperatures expected in ITER. It is insensitive to  $\psi$  and reaches its maximum for circularly polarized incident light.<sup>9</sup> For a conventional Thomson scattering geometry with scattering angle  $\theta \simeq 90^\circ$ , the degree of depolarization of circular polarized incident light is about five times larger ( $\sim 20\% - 25\%$ ). The absolute maximum  $D_{max} \sim 95\%$  is reached at  $\psi = 90^\circ$  for elliptically polarized incident light (see Fig. 1). This extreme regime corresponds to very small scattered power and results in large error bars for polarization-based  $T_e$  measurements. More practical cases of circular and linear incident polarizations are illustrated in Fig. 4 for conventional TS diagnostics at three scattering angles. Although circular incident polarization yields stronger depolarization of scattered radiation, rigorous minimization of the error bars shows that linear incident polarization is preferential for polarization-based diagnostics.

### III. INTERFEROMETRY AND POLARIMETRY

The ITER TIP system is designed for line-integrated tangential plasma density measurement from both traditional interferometry and Faraday-effect polarimetry.<sup>3</sup> Faraday-effect polarimetry can be used to independently measure the plasma density, since the toroidal magnetic field is known, or to correct the interferometer for fringe jumps. In a cold plasma, the interferometric phase  $\Phi$  and the Faraday rotation angle of polarization  $\psi_F$  are proportional to the line integral of the electron density and the line integral of the electron density multiplied by the parallel component of the magnetic

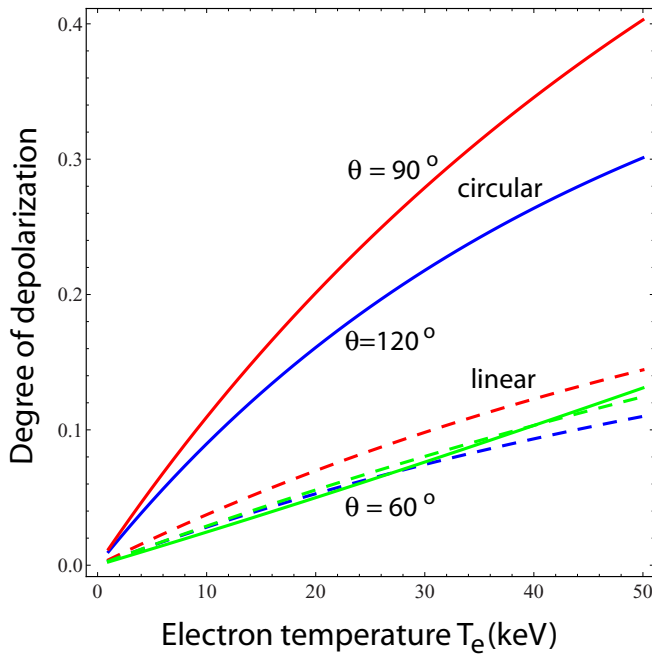


FIG. 4. Depolarization degree vs  $T_e$  for three scattering angles:  $60^\circ$  (green),  $90^\circ$  (red), and  $120^\circ$  (blue) (solid lines: circular polarization at  $\chi = 45^\circ$ ; dashed lines: linear polarization at  $\psi = \chi = 0$ ).

field, respectively. For the ITER TIP system parameters,  $n \simeq 10^{20} m^{-3}$ ,  $B_{\parallel} \simeq 5.3T$ ,  $L \simeq 21m$ ,  $\lambda = 10.6\mu m$ ,  $\Phi^{(cold)} \simeq 63$  rad, and  $\psi_F \simeq 19^\circ$ . The ITER PoPola diagnostic is based on Faraday and Cotton-Mouton effects for laser beams launched in the poloidal plane. It will provide a unique method of internal magnetic field and current profile measurement, in addition to electron density.<sup>4</sup> With propagation largely perpendicular to the magnetic field, the Cotton-Mouton effect becomes significant and leads to a change in the ellipticity angle  $\chi$ . For the PoPola system parameters,  $n \simeq 10^{20} m^{-3}$ ,  $B_{\perp} \simeq 5.3T$ ,  $L \simeq 8m$ , and  $\lambda = 118\mu m$ , the induced ellipticity of radiation initially linearly polarized at  $45^\circ$  to  $\mathbf{B}_{\perp}$  is given by  $\chi^{(cold)} \simeq 52^\circ$ .

These results for the I/P characteristics are derived from a cold plasma model. One source of error is finite electron temperature effects neglected in the cold plasma dispersion relation. Thermal corrections are proportional to  $\tau = T_e/m_e c^2$  and are small at  $T_e \sim 1$  keV, but become sizable at  $T_e \geq 10$  keV. There are two physically different sources of thermal corrections that are comparable in magnitude but contribute with opposite sign: non-relativistic Doppler-like effects, and the relativistic electron mass dependence on velocity. The effects of finite electron temperature were addressed in the non-relativistic limit in Ref. 11. Our reevaluation of this problem demonstrated that weakly relativistic effects are equally important and cannot be ignored.<sup>2</sup> The relativistic effects turn out to be stronger than the non-relativistic contributions for interferometry and Faraday-effect polarimetry. They change the sign of the non-relativistic corrections for the interferometric phase and Faraday rotation angle, and reduce the magnitude of the non-relativistic thermal correction for the Cotton-Mouton effect. At  $T_e = 25$  keV, the resulting values of the interferome-

try, FR, CM effects relative to their values in cold plasma are, respectively,  $-7.5\%$ ,  $-10\%$ , and  $+22.5\%$ , while the non-relativistic model yields overestimated values,  $+5\%$ ,  $+15\%$ , and  $+60\%$ , correspondingly.

For formal analysis of the problem, we developed an iterative technique for solving the relativistic Vlasov kinetic equation. The key element of the method is expansion in powers of  $Y = \omega_{ce}/\omega \ll 1$  instead of integration over azimuthal angle in the velocity space. This avoids the use of a complicated Bessel function series representation. Instead, expansion is performed by successive differentiations of simple standard trigonometric functions. The final result is in the analytic form of a double power series expansion of the dielectric tensor in  $Y \ll 1$  and  $\tau \ll 1$  to any desirable order. The validity of the method has been proven computationally by comparison with the ray-tracing numerical code GENRAY of Ref. 12. The theoretical predictions have also been confirmed by direct measurements on the JET tokamak.<sup>13</sup> Data collected from high- $T_e$  JET discharges demonstrated good agreement with the relativistic theory and disagreement with the cold plasma and non-relativistic models. These were the first experimental observations of relativistic effects in plasma polarimetry.

The model which adequately describes evolution of polarization of the EM wave in a nonuniform plasma and magnetic field is based on the Stokes vector equation<sup>14</sup>

$$\frac{ds}{dz} = \Omega \times s,$$

where the three-component unit Stokes vector  $\mathbf{s}$  is defined in Sec. II,  $z$  is a coordinate along the propagation direction and the spatially varying angular velocity vector  $\Omega(z)$  depends on plasma and magnetic field parameters. The  $\Omega_1$  and  $\Omega_2$  components are responsible for the CM effect and  $\Omega_3$  describes the Faraday rotation. This equation takes into account coupling between FR and CM effects due to the quasi-perpendicular directions of the optical paths in ITER PoPola system. The Stokes vector equation allows us to address the issue of the coupling while properly accounting for the thermal effects. Linear in  $\tau$  temperature corrections were incorporated in this model in Ref. 2. The precision of this lowest-order linear in  $\tau$  model may be insufficient; using the same iterative technique we recently constructed a more sophisticated model<sup>15</sup> with  $\tau^2$ -order corrections to satisfy the accuracy requirements for the ITER TIP and PoPola systems. The corresponding expression for  $\Omega$  is presented in Ref. 15. We illustrate here the structure of linear and  $\tau^2$  corrections by using the interferometric phase  $\Phi$  as an example. Relative deviation of  $\Phi$  from its cold plasma value  $\Phi^{(cold)}$  is caused by the thermal effects and reads

$$\frac{\Delta\Phi^{(T)}}{\Phi^{(cold)}} = \left( -\frac{3}{2} \int \frac{n_e T_e}{m_e c^2} dz + \frac{15}{8} \int \frac{n_e T_e^2}{m_e^2 c^4} dz \right) / \int n_e dz.$$

For the ITER TIP system with a  $\text{CO}_2$  laser at  $\lambda = 10.6\mu m$ , a central viewing channel optical path length of 21 m, a plasma density of  $10^{20} m^{-3}$ , and  $T_e = 25$  keV, the linear thermal correction to the interferometric phase is large ( $\sim 270^\circ$ ), and the quadratic correction is also significant ( $\sim 17^\circ$ ). With the  $\tau^2$ -model and  $T_e$  known from Thomson scattering, finite  $T_e$

effects can be rapidly and accurately calculated. This capability is particularly important for fast real-time feedback corrections in ITER.

New effects come into play when the electron distribution function develops an anisotropy. This could be caused by a large mean electron drift velocity  $U_{\parallel e}$  (parallel equilibrium current), an enhanced effective perpendicular temperature  $T_{\perp}$  in ECRH heated plasmas, or a large effective parallel temperature  $T_{\parallel}$  due to LH current drive. The corresponding vector  $\mathbf{\Omega}$  in the Stokes equation can be presented as a sum of three contributions  $\mathbf{\Omega} = \mathbf{\Omega}^{(0)} + \mathbf{\Omega}^{(B)} + \mathbf{\Omega}^{(U)}$ . The first term does not depend on the magnetic field and describes the effect of birefringence caused by the temperature anisotropy

$$\mathbf{\Omega}^{(0)} = (1 - N^2) \frac{\omega X (T_{\parallel} - T_{\perp})}{2c m_e c^2} \begin{pmatrix} 1 \\ 1 \\ 0 \end{pmatrix} \propto \frac{\omega X^2 (T_{\parallel} - T_{\perp})}{2c m_e c^2}$$

where  $X = \omega_{pe}^2/\omega^2$ . It results in evolution of the polarization ellipse similar to the usual “magnetic” Cotton-Mouton effect. The magnitude of the effect is strongly reduced by almost exact cancellation of the relativistic and non-relativistic Doppler-like contributions expressed, correspondingly, by the unity and  $N^2$  term in the factor  $(1 - N^2) \propto X$ . The residual small effect ( $\propto X^2$ ) exceeds “magnetic” Cotton-Mouton effect in high- $\beta$  plasmas. In the low- $\beta$  case, it can be a potential source of 1% – 3% errors for the ITER PoPola diagnostic system.

The second term,  $\mathbf{\Omega}^{(B)}$ , describes the generalization of linear in  $\tau$  isotropic results to the case of non-Maxwellian anisotropic distributions. These results can be used for correction of the interpretation errors in fusion plasmas with non-Maxwellian distributions generated by ECRH and other RF sources such as EC and LH current drive

$$\mathbf{\Omega}^{(B)} = \Omega^{(c)} + \cos 2\alpha \frac{(T_{\parallel} - T_{\perp})}{2m_e c^2} \begin{pmatrix} 10\Omega_1^{(c)} \\ 10\Omega_2^{(c)} \\ 3\Omega_3^{(c)} \end{pmatrix} + \frac{1}{2m_e c^2} \times \begin{pmatrix} (5T_{\parallel} + 4T_{\perp})\Omega_1^{(c)} \\ (5T_{\parallel} + 4T_{\perp})\Omega_2^{(c)} \\ -(3T_{\parallel} + T_{\perp})\Omega_3^{(c)} \end{pmatrix}, \quad \Omega^{(c)} = \frac{\omega}{2c} \begin{pmatrix} XY^2 \sin^2 \alpha \cos 2\beta \\ XY^2 \sin^2 \alpha \sin 2\beta \\ 2XY \cos \alpha \end{pmatrix},$$

where  $\alpha$  and  $\beta$  are spatially varying angles of the magnetic field  $\mathbf{B}$  in a spherical reference frame with  $\mathbf{z} \parallel \mathbf{k}$  ( $\alpha$  is the angle between  $\mathbf{k}$  and  $\mathbf{B}$  and  $\beta$  is the azimuth angle in the  $x, y$  plane between  $\mathbf{x}$  and  $\mathbf{B}_{\perp}$ ).

Motion of the electron component as a whole (equilibrium current) can be treated in terms of the Fizeau effect, that is, the phase velocity of electromagnetic waves depends on whether they propagate in a moving or stationary medium. This suggests a new interferometric scheme for measuring the equilibrium current density by comparing the phases of two counter-propagating laser beams. This method was proposed to measure the line integrated poloidal electron current.<sup>16</sup> Lorentz-transformation based calculations for a plasma slab moving with velocity  $U_e$  orthogonal to the slab boundary predicted a measurable interferometric phase shift  $\Delta\phi \simeq (\omega/c)(U_e/c)XL \simeq 2^\circ$  with a FIR laser at  $\lambda = 432\mu\text{m}$ , a

central viewing optical path length of 1 m, a plasma density of  $1.5 \times 10^{19} \text{m}^{-3}$ , and current density  $\sim 1.5 \text{MA/m}^2$ . A more sophisticated slab model with the velocity vector oriented arbitrarily with respect to the slab surface showed that in a cold non-magnetized plasma, only the velocity component perpendicular to the plasma density isosurface can be measured.<sup>17</sup> For the parallel component, which is of the main interest for current density diagnostics, the Fizeau effect cancels out due to specific scaling of plasma refractive index on frequency.<sup>18</sup> This can also be seen from the structure of the isotropic electron dielectric tensor which is insensitive to the Doppler shift of the frequency  $\mathbf{k} \cdot \mathbf{U}$  caused by the mean electron velocity.

In the presence of a magnetic field, the non-magnetized electron dispersion relation is modified. Calculating the electron dielectric tensor, we found new physical properties of the Fizeau effect. They appear in the form of birefringence of electromagnetic waves due to the combined action of the magnetic field and electron drift velocity. The Fizeau effect is recovered in a magnetized plasma because the Doppler shifted frequencies do not cancel in magnetic field dependent elements of the dielectric tensor. Evolution of the wave polarization caused by parallel electron equilibrium current is described by the Stokes vector equation with the vector  $\mathbf{\Omega}^{(U)}$

$$\mathbf{\Omega}^{(U)} = \frac{\omega U_{\parallel e}}{c^2} \begin{pmatrix} XY^2 \cos \alpha \sin^2 \alpha \cos 2\beta \\ XY^2 \cos \alpha \sin^2 \alpha \sin 2\beta \\ XY \cos 2\alpha \end{pmatrix}.$$

This may open new possibilities for diagnosis or measurements of the parallel equilibrium current (Fizeau polarimetry).<sup>19</sup>

#### IV. SUMMARY

Using the theoretical model for TS polarization allows us to optimize the experimental setup for polarization-based  $T_e$  measurements. For optimization, the diagnostic error bars are calculated and minimized with respect to polarization characteristics of the incident light  $\psi$  and  $\chi$  and scattering angle  $\theta$ . In the general case of elliptically polarized incident light, four Stokes vector components of the scattered light should be measured. Modifying the standard scheme of six measurable intensities,<sup>10</sup> we select four independent intensities  $I_{\alpha}$  to determine  $\mathbf{S}^{(s)}$

$$S_0^{(s)} = I_{0^\circ} + I_{90^\circ}, S_1^{(s)} = I_{0^\circ} - I_{90^\circ},$$

$$S_2^{(s)} = I_{0^\circ} + I_{90^\circ} - 2I_{135^\circ}, S_3^{(s)} = I_{0^\circ} + I_{90^\circ} - 2I_{135^\circ}^{\pi/2}.$$

Three of them are measured after the light is separated by beamsplitters and transmitted by three polarizers that select linear polarization at the azimuth angles  $0^\circ$ ,  $90^\circ$ , and  $135^\circ$  with respect to the perpendicular to the scattering plane. The fourth channel contains a quarter-wave plate to create  $\pi/2$  retardation of the in-plane component before the light is transmitted by the  $135^\circ$  polarizer. The degree of depolarization measurement error,  $\sigma_D$ , is related to the error on each of the

statistically independent intensity measurements  $\sigma_{I_\alpha}$

$$\sigma_D^2 = \sum_{\alpha} \left( \frac{\partial D}{\partial I_\alpha} \right)^2 \sigma_{I_\alpha}^2,$$

where the intensity measurement errors are determined by Poisson statistics such that  $\sigma_{I_\alpha}^2 \propto I_\alpha$ . The relative error in the electron temperature measurement,  $\sigma_{T_e}/T_e = \sigma_D(T_e \partial D / \partial T_e)^{-1} = W / (\sqrt{Q} T_e \partial D / \partial T_e)$ , is presented by a product of two universal functions  $W(\psi, \chi, \theta, T_e)$  and  $(\partial D / \partial T_e)^{-1}(\psi, \chi, \theta, T_e)$  with a scaling factor  $1/\sqrt{Q}$  which does not depend on the polarization variables ( $Q$  is effectively proportional to the total number of scattered photons). The factorization allows us to perform minimization of  $\sigma_{T_e}$  analytically for the full range of incident polarizations, scattering angles, and electron temperatures. Although Fig. 4 shows that at  $\theta = 90^\circ$  and  $\theta = 120^\circ$ , the derivative  $\partial D / \partial T_e$  is the largest for circular polarization, fast growth of  $W$  in this parameter range determines the overall minimum of the error bars at linear incident polarization with  $\chi = \psi = 0$ . This proves that the regime of linear polarization with  $\psi = 0$  is optimal not only because of the convenience of two-channel measurements but due to intrinsic polarization properties of Thomson scattered radiation. More detailed analysis is presented in Ref. 20. At  $\theta \sim 90^\circ$  and  $T_e > 9$  keV, the error bars are less than 5%, and less than 2% above 23 keV making polarization-based diagnostics competitive with standard spectrum-based measurements.

For ITER polarimetry (FR and CM) and interferometry measurements, it is proposed to use retroreflection of the I/P probing laser beams so that the beam enters and exits through the same port. With retroreflection, the FR and CM effects on the input and return paths are additive if the retroreflection is performed through an odd number of reflections and subtractive if the number of reflections is even.<sup>21</sup> Evolution of polarization resulting from the mean electron velocity and described by  $\Omega^{(U)}$  exhibits an opposite response and is additive in the case of an even number of reflections. If polarization effects are small enough, using the roof-top reflector (RTR) allows us to eliminate contributions from magnetic FR and CM effects described by the  $\Omega^{(B)}$  vector and detect the signal determined by the pure  $\Omega^{(U)}$  effect. Using FIR laser wavelength  $\lambda = 432 \mu\text{m}$  with parallel propagation ( $\alpha = 0$ ) along the central viewing cord of ITER TIP system and double-passed retro-reflection from RTR, yields the angle of rotation of polarization  $\psi_U \sim 15^\circ$  at  $U_{\parallel e}/c \sim 5 \times 10^{-4}$ . Another effect is predicted in the case of quasi-perpendicular propagation  $\alpha = 90^\circ$ . Then, the magnetic Fara-

day effect cancels out while rotation of the polarization plane still takes place due to birefringence described by  $\Omega_3^{(U)}$  term with  $\cos 2\alpha = -1$ .

## ACKNOWLEDGMENTS

This material is based on work supported by the U.S. Department of Energy Office of Science, Office of Fusion Energy Sciences under Award Nos. DE-FC02-05ER54814, DE-FG02-01ER54615, the U.S. NSF Cooperative Agreement No. PHY-0821899 Center for Magnetic Self-Organization in Laboratory and Astrophysical Plasmas and the U.S. ITER Project Office.

- <sup>1</sup>I. H. Hutchinson, *Principles of Plasma Diagnostics* (Cambridge University Press, 2002), p. 440.
- <sup>2</sup>V. V. Mirnov, W. X. Ding, D. L. Brower, M. A. Van Zeeland, and T. N. Carlstrom, *Phys. Plasmas* **14**, 102105 (2007).
- <sup>3</sup>M. A. Van Zeeland, R. L. Boivin, D. L. Brower, T. N. Carlstrom, J. A. Chavez, W. X. Ding, R. Feder, D. Johnson, L. Lin, R. C. O'Neill, and C. Watts, *Rev. Sci. Instrum.* **84**, 043501 (2013).
- <sup>4</sup>R. Imazawa, Y. Kawano, and Y. Kusama, *Nucl. Fusion* **51**, 113022 (2011).
- <sup>5</sup>F. Orsitto and N. Tartoni, *Rev. Sci. Instrum.* **70**, 798 (1999).
- <sup>6</sup>J. Sheffield, D. H. Froula, S. H. Glenzer, and N. C. Luhmann, *Plasma Scattering of Electromagnetic Radiation*, 2nd ed. (Academic Press, 2011), p. 520.
- <sup>7</sup>S. E. Segre and V. Zanza, *Phys. Plasmas* **7**, 2677 (2000).
- <sup>8</sup>R. E. Pechacek and A. W. Trivelpiece, *Phys. Fluids* **10**, 1688 (1967).
- <sup>9</sup>V. V. Mirnov, D. L. Brower, D. J. Den Hartog, W. X. Ding, J. Duff, and E. Parke, *Proceedings of 24th International Conference on Fusion Energy*, ITR/P5-32, San Diego, CA (IAEA, Vienna, 2012).
- <sup>10</sup>M. Born and E. Wolf, *Principles of Optics*, 3rd ed. (Pergamon Press, 1965), p. 808.
- <sup>11</sup>S. E. Segre and V. Zanza, *Phys. Plasmas* **9**, 2919 (2002).
- <sup>12</sup>A. P. Smirnov, R. W. Harvey, and K. Kupfer, *Bull. Am. Phys. Soc.* **39**, 1626 (1994).
- <sup>13</sup>O. P. Ford, J. Svensson, A. Boboc, D. C. McDonald, and JET EFDA Contributors, *Plasma Phys. Controlled Fusion* **51**, 065004 (2009).
- <sup>14</sup>S. E. Segre, *Plasma Phys. Controlled Fusion* **41**, R57 (1999).
- <sup>15</sup>V. V. Mirnov, D. L. Brower, D. J. Den Hartog, W. X. Ding, J. Duff, and E. Parke, *Nucl. Fusion* **53**, 113005 (2013).
- <sup>16</sup>D. L. Brower, W. X. Ding, B. H. Deng, M. A. Mahdavi, V. Mirnov, and S. C. Prager, *Rev. Sci. Instrum.* **75**, 3399 (2004).
- <sup>17</sup>V. V. Mirnov, D. L. Brower, and W. X. Ding, *Collection of Abstracts of International Sherwood Fusion Energy Conference*, Boulder, CO (2008) ([http://sherwood.colorado.edu/Uploads/MIRNOV\\_\\_onpossib3101\\_10.pdf](http://sherwood.colorado.edu/Uploads/MIRNOV__onpossib3101_10.pdf)).
- <sup>18</sup>I. Lerche, *Am. J. Phys.* **43**, 910 (1975).
- <sup>19</sup>V. V. Mirnov, D. L. Brower, D. J. Den Hartog, W. X. Ding, J. Duff, and E. Parke, submitted to *AIP Proceedings of International Conference on Fusion Reactor Diagnostics*, Varenna, Italy (AIP Publishing, 2014), vol. 1609.
- <sup>20</sup>E. Parke, V. V. Mirnov, and D. J. Den Hartog, *Proceedings of the 16th International Symposium on Laser-Aided Plasma Diagnostics* (Madison, WI, 2013); *J. Instrum.* **9**, C02030 (2014).
- <sup>21</sup>S. E. Segre and V. Zanza, *Plasma Phys. Controlled Fusion* **50**, 105006 (2008).